PAPER

Dynamics of recombination in viscous electron–hole plasma in a mesoscopic GaAs channel

To cite this article: Yu A Pusep *et al* 2023 *J. Phys. D: Appl. Phys.* **56** 175301

IOP Publishing Journal of Physics D: Applied Physics
J. Phys. D: Appl. Phys. **56** (2023) 175301 (8pp) https://doi.org/10.1088/1361-6463/acba2a

Dynamics of recombination in viscous electron–hole plasma in a mesoscopic GaAs channel

Yu A Pusep[1,*], M D Teodoro[2], M A T Patricio[1], G M Jacobsen[2], G M Gusev[3], A D Levin[3] and A K Bakarov[4]

[1] São Carlos Institute of Physics, University of São Paulo, PO Box 369, 13560-970 São Carlos, SP, Brazil
[2] Departamento de Física, Universidade Federal de São Carlos, 13565-905 São Carlos, São Paulo, Brazil
[3] Institute of Physics, University of São Paulo, 135960-170 São Paulo, SP, Brazil
[4] Institute of Semiconductor Physics, 630090 Novosibirsk, Russia

E-mail: pusep@ifsc.usp.br

Received 13 October 2022, revised 25 January 2023
Accepted for publication 8 February 2023
Published 15 March 2023

Abstract

The recombination dynamics are studied in viscous electron–hole plasma, consisting of electrons and photo-generated heavy and light holes, formed in the high-mobility mesoscopic GaAs channel. It is shown that an increase in the pump power reduces the concentration and mobility of background electrons, which, in turn, slows down their recombination with photogenerated holes. At a critical pump power, the recombination time begins to decrease, which is a consequence of the transition of a viscous electron–hole plasma from the hydrodynamic regime to the Drude diffusive regime. The observed transition occurs when the scattering of electrons with disorder begins to dominate over electron–electron scattering, which leads to the transformation of an inhomogeneous Poiseuille charge flow into a homogeneous diffusion flow. As a result, an optical analogue of the Gurzhi effect has been found.

Keywords: quantum well, photoluminescence, hydrodynamics, recombination, diffusion

(Some figures may appear in colour only in the online journal)

1. Introduction

Minimization of semiconductor devices leads to the fact that the validity of the drift-diffusion equations becomes doubtful and a more accurate description of the electrical properties of devices is required [1]. In order to improve electric characterization of tiny semiconductor devices, the hydrodynamic approach has been successfully applied to correlated ($r_s \gtrsim 1$) high-mobility two-dimensional (2D) electron systems formed in graphene and GaAs quantum wells (QW) (see for example [2–5]), where the dominant role of electron–electron scattering ($l_{ee} << l_p$, where l_{ee} and l_p are the electron mean free paths associated with electron–electron scattering and momentum relaxation, respectively) ensures the hydrodynamic response of electrons. Under such conditions, the hydrodynamic behavior of electrons was predicted in [6], and the first experimental observation of hydrodynamic electron Poiseuille flow by differential resistance measurements of electrostatically determined 2D wires formed in GaAs/AlGaAs QW was claimed in [7, 8]. Later [9, 10] it was reported that, most likely, one-dimensional diffusion of charge carriers associated with a mixed ballistic-hydrodynamic flow is detected in these experiments. The existence of a viscous electron fluid was first stated in [11] based on an analysis of previously published measurements of the temperature-dependent giant negative magnetoresistance of 2D electrons in high-quality GaAs QWs,

* Author to whom any correspondence should be addressed.

which initiated a significant number of publications in this field [12–17].

Furthermore, the hydrodynamic properties of dense electron–hole plasma were predicted in semiconductors in which the electron–electron, electron–hole and hole–hole collisions dominate over the collisions of electrons and holes with disorder [18]. Diffusion of photogenerated holes was recently studied in [19] by measuring photocurrent (PC) in viscous electron gas formed in high-mobility mesoscopic GaAs channel where hydrodynamics governs the transport properties of a bipolar electron–hole plasma. The PC was measured under specific conditions when, after photogeneration in AlGaAs barriers, holes tunneled into the GaAs QW, where they recombined with background electrons, which caused a decrease in the electron concentration and, consequently, in the PC. In this case the injection of holes leads to the formation of a hydrodynamic three-component mixture consisting of electrons and photo-generated heavy and light holes. In this paper, we report on the investigation of the recombination dynamics in such a system. The evidence of injection of photogenerated holes from the barriers of the QW and proof of the contribution of heavy and light holes to the formation of three-component viscous electron–hole plasma are presented. Moreover, a remarkable behavior of the recombination time with increasing pump power is found: first, the recombination time increases due to a decrease in the electron mobility, and then, at a certain pump power, the increasing electron scattering transforms the inhomogeneous Poiseuille charge flow of a viscous electron–hole plasma into a normal nearly uniform Drude diffusion flow, resulting in a decrease in the recombination time. Such a change in the character of the charge flow becomes possible to observe due to the presence of channel boundaries. Near the boundaries, recombination occurs faster than in the middle of the mesoscopic channel. The uniform charge flow increases the fraction of photogenerated holes at the channel boundary, thereby increasing the rate of their recombination. The observed variation in the character of the charge flow, which manifests itself in the corresponding change in the average recombination time, indicates a transition from viscous to diffusive charge flow.

Moreover, the importance of the boundaries in mesoscopic devices was recently pointed out in [17, 20]. The boundary conditions are not universal and depend on the details of the solid surface, which strongly affects the charge flow dynamics in mesoscopic devices. In this case, knowledge of the precise nature of the boundary conditions at various interfaces is of great practical importance. In this way, the presented study of the recombination dynamics makes it possible to reveal the nature of the boundary interfaces of a certain mesoscopic device and, thus, to describe the details of the corresponding charge flow.

2. Experimental details

A hydrodynamic 2D electron gas was built in a single GaAs/AlGaAs QW 14 nm thick, grown on (100)-oriented GaAs substrate by a molecular beam epitaxy. The experiments were carried out on a mesoscopic channel formed by a multi-terminal Hall bar structure with an active area width of 5 μm and a length of 100 μm. The sheet electron density and the mobility measured by standard Hall measurements at the temperature of 1.4 K were 4.8×10^{11} cm^{-2} and 1.0×10^{6} cm^2 V^{-1} s^{-1}, respectively, which leads to the interaction parameter r_s close to unity. In this case the hydrodynamic regime was considered in [16]. Scanning PC microscopy experiments were performed at the temperature 3.7 K using a helium closed cycle cryostat Attocube/Attodry1000. An electrically connected sample was placed on top of a *x*–*y*–*z*nanopositioner stack, which allows for precise positioning of the laser beam focused by an aspheric objective (NA = 0.64) along the channel. The PC measurements were carried out with a Keithley 2400 source meter with optical excitation by diode lasers emitting at the energies 1.7 eV and 2.33 eV. Excitation at 1.7 eV generates electron–hole pairs in the GaAs QW, but not in the barrier, whose gap is about 1.8 eV, while excitation energy of 2.33 eV leads to electron–hole excitation both in the QW and in the barrier. Photoluminescence (PL) and the time-resolved PL measurements were performed with the same Pico Quant/LDH Series diode laser emitting continuous radiation (PL) and 80 MHz pulses at 730 nm (1.7 eV) with a pulse duration of 70 ps (time-resolved PL). The temporal resolution of the setup used is 100 ps. PL emission was dispersed by a 75 cm Andor/Shamrock spectrometer and the PL transients were detected by a PicoQuant Hybrid PMT detector triggered triggered with a time correlated single photon PicoQuant/PicoHarp 300 counting system. The laser instrument response function (IRF), which is responsible for the temporal resolution of the setup was measured as a transient process of reflected laser light measured at the laser energy (shown in the inset to figure 4).

The process of recombination of holes injected into the channel with background electrons is schematically shown in figure 1(a). Holes are photogenerated in the dark red region from where they diffuse through the channel. The white area in figure 1(a) shows a decrease in the intensity of injected holes as they move away from the laser spot, while the blue region shows the intensity of the background electrons. The calculated energy structure of the studied here sample is depicted in figure 1(b) where the relevant electron and hole levels are shown. The only lowest energy fundamental confined level is found in the conduction band below the Fermi energy. Optical excitation in the region of barriers leads to spatial separation of photogenerated electrons and holes due to the built-in electric field. As a consequence, photogenerated holes tunnel into the QW, where their recombination with background doping electrons causes a decrease in the electron concentration.

Since the hydrodynamic behavior of electrons in GaAs is expected in a narrow temperature range at $T \lesssim 35$–40 K, the sample temperature upon laser excitation is an important issue. Direct temperature control of a mesoscopic sample is difficult due to its small size, which is smaller than a temperature sensor. In this case, we used the shape of the PL spectra to estimate the temperature of the mesoscopic channel at the

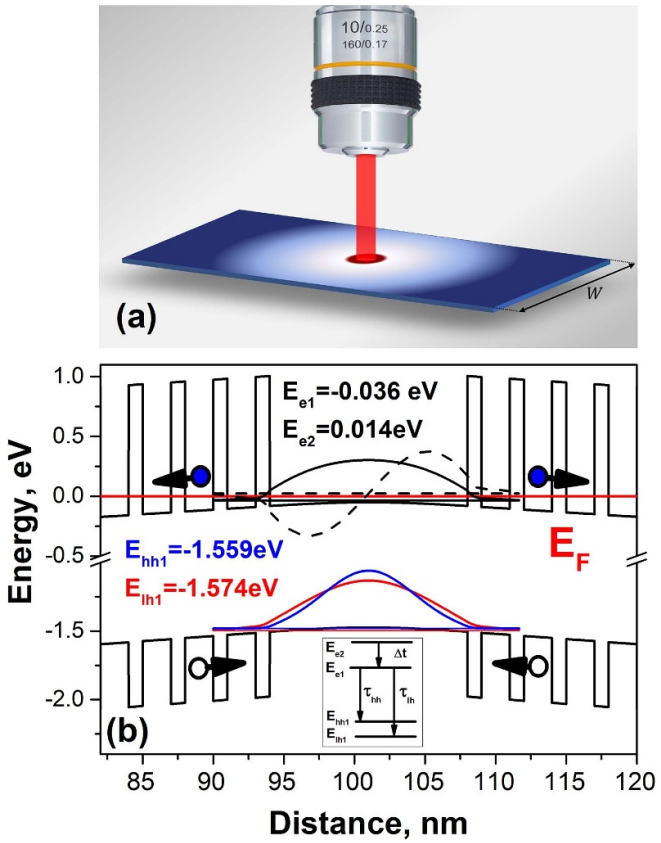

Figure 1. (a) Scheme of diffusion and recombination processes in a mesoscopic GaAs channel of width W after the injection of photogenerated holes into the dark red region. The white and blue regions show the densities of injected holes and background electrons, respectively. (b) Calculated energy structure of the GaAs/AlGaAs quantum well. Fermi energy is used as an energy reference. The inset shows schematic representation of the considered transitions.

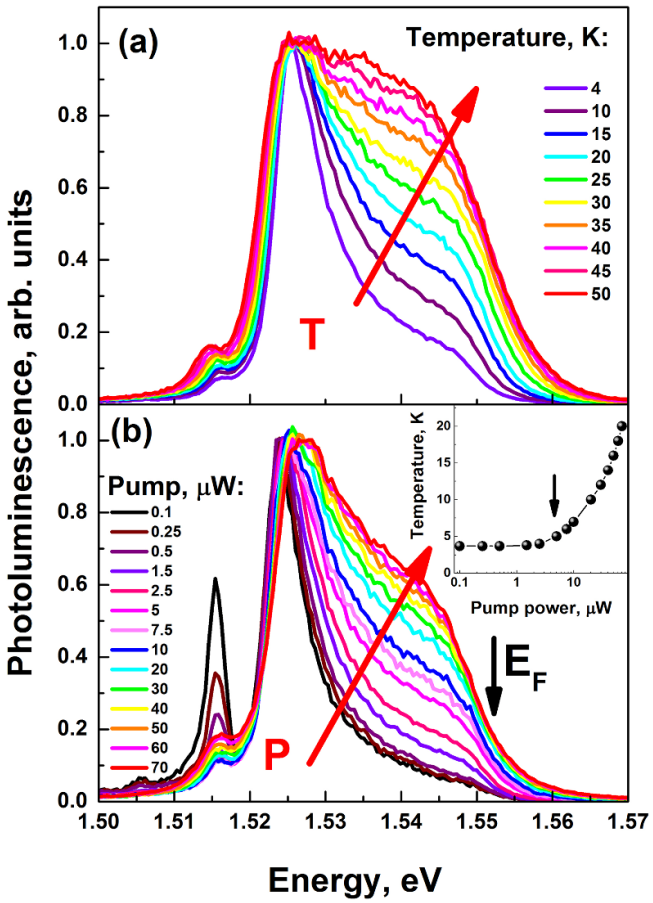

Figure 2. Normalized PL intensity measured with an excitation energy of 1.7 eV in the mesoscopic GaAs channel as a function of temperature at the average pump power 5 μW (a) and as a function of the pump power P at $T = 3.7$ K (b). The inset shows the temperature at the laser excitation point. The arrow in the inset indicates the average pump power P used during PC measurements.

laser excitation point. The PL spectra measured as a function of temperature and pump power are shown in figure 2.

PL emission is observed in the energy range between the band gap and the Fermi level energy. The Fermi energy extracted from the PL spectra (about 32 meV) is found in good agreement with the Fermi energy determined by the magnetotransport measurements (30 meV). The weak peak around 1.515 eV is due to recombination involving DX centers. It is important that, in the n-type QW under study, the shape of the PL spectrum is affected by the occupation of the states of the valence band by minority photogenerated holes. Not all electrons below the Fermi energy contribute equally to recombination with photogenerated holes. Only a small fraction of electrons near the bottom of the conduction band is available for this process, since at low temperatures only a small number of hole states at the top of the valence band are occupied. Therefore, the strong maximum near the band edge energy is caused by the recombination of electrons with photogenerated holes, which tend to accumulate at the extremum of the valence band. Such effect of the thermal distribution of the minority carriers on the shape of PL spectra was studied in [21]. With increasing temperature, the energy distribution of photogenerated holes over the valence band becomes more uniform, which leads to the disappearance of the PL maximum. Thus, the sample temperature can be determined by comparing the PL spectra shown in figures 2(a) and (b), respectively. Temperature of the sample at the laser excitation point obtained in this way is shown in the inset to figure 2(b). The measurements performed in the present study were carried out at an average laser pump power of 5 μW, indicated by an arrow in the inset to figure 2(b).

3. Results and discussion

The PC measured in the mesoscopic channel as a function of the distance between the laser spot and PC probes 1 and 2 (diffusion profile) at various excitation energies is shown in figure 3(a). Technical details of the PC measurements can be found in [19] . Excitation of electron–hole pairs at an energy of 2.33 eV above the barrier gap reveals a minimum of the PC, while it is not detected at an excitation energy of 1.7 eV below the barrier gap, that is in the QW. The observed PC minimum is due to the diffusion of photogenerated holes followed by

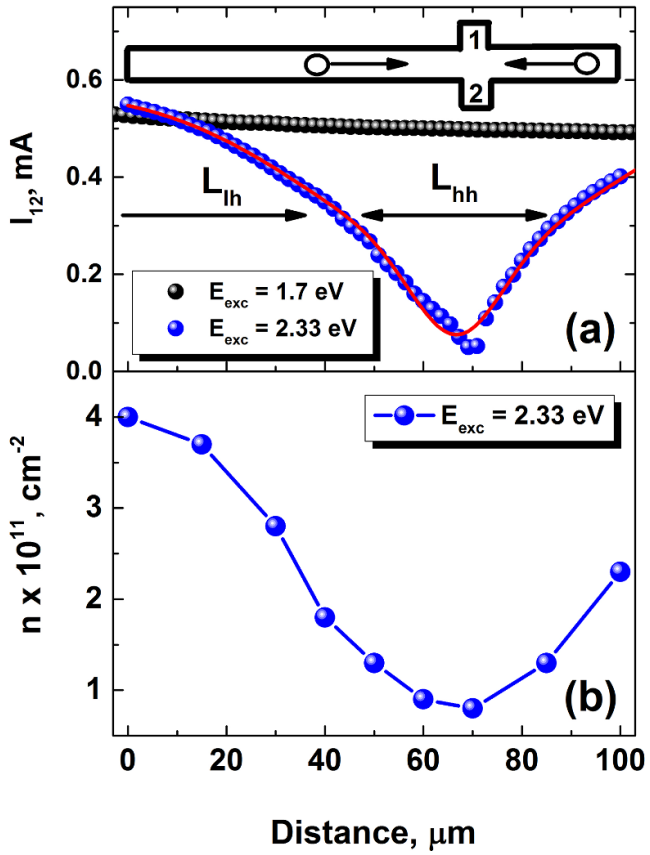

Figure 3. (a) Photocurrent measured with the collecting photocurrent probes 12 in a mesoscopic GaAs channel at $T = 3.7$ K, at an excitation energy of 2.33 eV above the barrier gap (blue circles) and at an excitation energy of 1.7 eV below the barrier gap (black circles). The red line is calculated according to equation (1). The ranges in which heavy and light holes make the greatest contribution are indicated by horizontal arrows. (b) Electron concentration measured as a function of the laser spot position.

their combination with background electrons (the doping electrons in the absence of photo-excitation), which reduces the PC at the collecting contacts. As demonstrated in [19], this diffusion profile is well described by the diffusion of heavy and light holes. Under these conditions, the PC is determined by the total electron concentration which can be calculated as the difference between the concentrations of the background electrons n_0 and photogenerated holes according to the expression:

$$n(x) = n_0 - n_{\rm hh} \exp\left(-\frac{x^2}{4L_{\rm hh}^2}\right) - n_{\rm lh} \exp\left(-\frac{x^2}{4L_{\rm lh}^2}\right) \qquad (1)$$

where the second and third terms are associated with heavy and light holes arriving at the collecting probes, $n_{\rm hh(lh)}$ is the heavy hole (light hole) concentration, while $L_{\rm hh}$ and $L_{\rm lh}$ are the diffusion lengths of heavy and light holes, respectively. Due to the effective mass difference, heavy and light holes contribute near to and far from the collecting contacts, respectively. Then the PC as a function of distance can be calculated as $j_{\rm PC}(x) = en(x)v_{\rm F}$, where $v_{\rm F}$ is the Fermi velocity. Fitting the experimental PC diffusion profile shown in figure 3(a) using equation (1) gives good agreement and manifests itself in the simultaneous diffusion of heavy and light holes. In this way, the diffusion lengths of heavy and light holes are obtained, equal to 6.3 μm and 21.8 μm, respectively. In addition, the Hall electron concentration was measured as a function of the distance between Hall probes 1 and 2 and the laser spot (the excitation energy 2.33 eV). These data are shown in figure 3(b) and are consistent with the PC diffusion profile depicted in figure 3(a).

Of particular interest is the question of the homogeneity of the electron–hole plasma produced by laser excitation. A steady-state electron–hole plasma is present during the recombination time within an area determined by the corresponding diffusion length, while the electron density is a function of the distance to the laser spot. However, the electron shear viscosity is $\nu \sim v_{\rm F} l_{\rm ee}$, where $v_{\rm F}$ is the Fermi velocity, and thus depends on the electron density. For this reason, the viscosity of the investigated electron–hole plasma can be inhomogeneous. In such a case, the diffusion coefficient is not a constant and must be replaced by an average value, while the diffusion profile may not take on a Gaussian form. Nevertheless, good agreement between the experimental and calculated by equation (1) PC diffusion profiles suggests Gaussian diffusion with a constant diffusion length and, consequently, the inhomogeneity of the electron–hole plasma does not significantly affect the measured PC. The weak effect of a change in the electron concentration on the viscosity can be caused by the renormalization of the viscosity due to the corresponding changes in the electron-electron interaction [22].

Additional evidence of the contribution of heavy and light holes was obtained in the study of the recombination dynamics by time-resolved PL presented below. The PL transients were measured at the energy 1.7 eV below AlGaAs barrier excitations. Thus, electron–hole pairs were generated within the GaAs QW. The laser spot was placed in the region of the mesoscopic channel near the central line. In this case, the PL transients did not depend on the position of the laser spot along the channel.

The PL transients measured in the mesoscopic channel and in the region of the 2D GaAs QW are shown in figures 4 and 5, respectively. They clearly demonstrate a biexponential decay of the PL intensity. Such character of transient PL processes can be associated with individual contributions from the states of heavy and light holes, which imply slow transference between them in comparison with their rapid recombination with electrons.

The inset in figure 1(b) shows a simple model that considers the transitions of radiative recombination between the lowest energy electron confined level and the lowest energy confined level of heavy, or light holes, as well as transitions between the second and first confined levels in the conduction band. The time delay between the pump laser peak IRF and the sample response, shown in the lower inset to figure 4, indicates the presence of two levels in the conduction band, one of which at a higher energy fills the lower energy level.The transfer of electrons between these confined levels is responsible for the

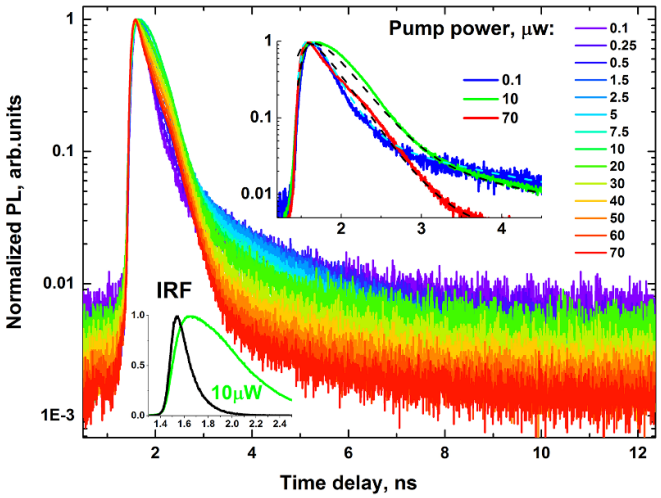

Figure 4. PL transients measured at $T = 3.7$ K in the mesoscopic GaAs channel at an excitation and emission energy of 1.7 eV and 1.54 eV, respectively, as a function of the pump power. The upper inset shows the PL transients measured at pump powers 0.1, 10, 70 μW with corresponding fits (dashed lines). The lower inset shows the PL transient measured at a pump power 10 μW together with the IRF (instrument response function) laser peak.

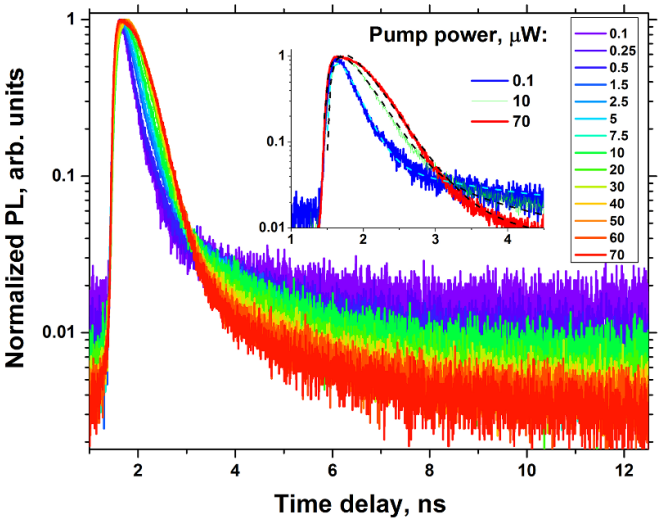

Figure 5. PL transients measured at $T = 3.7$ K in the region of the 2D GaAs QW at an excitation and emission energy of 1.7 eV and 1.54 eV, respectively, as a function of the pump power. The inset shows the PL transients measured at pump powers 0.1, 10, 70 μW with corresponding fits (dashed lines).

shown in the inset time delay [23].The same scheme is used for the recombinations of both heavy and light holes. The related rate equations can be written as:

$$\frac{dn_1}{dt} = \frac{n_2}{\Delta t} - \frac{n_1}{\tau_1} \tag{2}$$

$$\frac{dn_2}{dt} = \frac{n_0}{\tau_0} - \frac{n_2}{\Delta t} \tag{3}$$

where Δt—is the transference time between the confined electron levels, τ_1—holds either for the heavy hole (τ_{hh}) or light hole (τ_{lh}) radiative recombination time. The pump rate n_0/τ_0 responsible for population n_2 of the E_{e2} level is represented by the delta Dirac function. The integration of the rate equations yields the occupancies of the associated levels. Accordingly, the measured PL transients are due to the recombination of electrons in the states of the lowest energy first confined level E_{e1} below the Fermi level with heavy and light holes residing on the confined levels E_{hh1} and E_{lh1}, respectively. The second confined electron level E_{e2} above the Fermi level ensures that the first confined level is filled with photogenerated electrons. The laser excitation first pumps the E_{e2} level, and then the population of E_{e1}level from E_{e2} level takes place. Consequently, the population of E_{e1} level first increases, which leads to an increase in the PL intensity and a delay in the corresponding transient process. The lower inset to figure 4 depicts an enlarged transient scale, where the delay due to the relaxation of photogenerated electrons between the confined levels is clearly observed. The populations of the electron confined levels under consideration, which appear after laser pumping (at time $t > 0$), are:

$$n_1(t) = \frac{n_{01}\tau_1}{\tau_1 - \Delta t}\left[\exp\left(-\frac{t}{\tau_1}\right) - \exp\left(-\frac{t}{\Delta t}\right)\right] \tag{4}$$

$$n_2(t) = n_{02}\exp\left(-\frac{t}{\Delta t}\right) \tag{5}$$

where n_{01} and n_{02} are the corresponding initial concentrations. The inter-level transition time Δt and the recombination time τ_1 are responsible for the rise and decay of the PL intensity associated with the observed transition between the lowest energy electron confinement level and the heavy/light hole confinement level, respectively.

Since the electronic states involved in recombination occupy a wide range of energies below the Fermi level, the PL transients measured in the sample represent a superposition of transient processes caused by the recombinations of heavy and light holes with the electrons residing on the lowest energy level E_{e1}. In this case, the same recombination process takes place for the recombination of heavy and light holes with these electrons. Therefore, the resulting PL intensity is determined by the sum of two terms determined by equation (4), each of which refers to related to heavy holes (with the recombination time $\tau_1 = \tau_{hh}$) and light holes (with the recombination time $\tau_1 = \tau_{lh}$). Consequently, the measured PL decay is determined by the expression:

$$I_{PL}(t) = I_o + I_{hh}\exp\left(-\frac{t}{\tau_{hh}}\right) + I_{lh}\exp\left(-\frac{t}{\tau_{hh}}\right) - 2I_{12}\exp\left(-\frac{t}{\Delta t}\right) \tag{6}$$

where I_o, $I_{hh(lh)}$ and I_{12} are the background PL intensity, the PL intensity corresponding to the initial electron population of the E_{e1} level related to recombination with heavy(light) holes, and PL intensity corresponding to the initial amplitude of inter-level transitions in the conduction band, respectively. The PL intensity transients calculated in this way are used to fit the corresponding experimental PL transients.

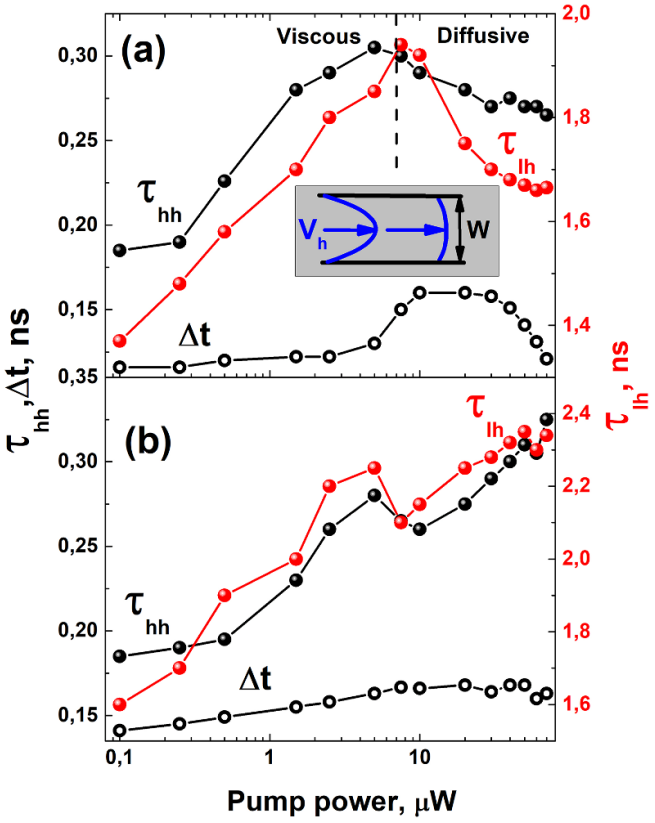

Figure 6. Recombination times of heavy and light holes τ_{hh} and τ_{hh}, respectively, and the transition time Δt between the levels confined in the conduction band and measured as a function of pump power in the channel (a) and in the area of 2D QW (b). The vertical dash line separates the viscous and diffusive regimes. The inset in the panel (a) shows the diffusion velocity profiles corresponding to low and high pump power, left and right images, respectively.

The PL transients measured as a function of the pump power in the mesoscopic channel and in the region of the 2D GaAs QW are shown in figures 4 and 5, respectively. The presented results unambiguously demonstrate that in the channel the characteristic decay time passes through a maximum, while in the region of 2D QW it monotonically increases with increasing pump power. The best fits of typical PL decays are shown in the corresponding insets, while the recombination times τ_{hh} and τ_{lh} obtained as a function of the pump power are depicted in figure 6.

It should be noted that when obtaining data indirectly, by the fitting procedure, it is not possible to accurately determine the experimental errors. In this case, the errors are mainly related to the fitting procedure. Short times τ_{hh} and Δt determine the transient processes of the PL near its maximum, where the signal-to-noise ratio is large, while the long time τ_{lh} is determined by the transient range in which the signal-to-noise ratio is considerably lower. Therefore, typical fitting errors in determining short and long times are less than 0.5% and 5%, respectively. For example, in the case of the PL transients shown in the upper inset to figure 4, the recombination times τ_{hh}, τ_{lh} and Δt, obtained at a pump power 10 μW with corresponding errors, are 0.2950±0.0006, 1.91±0.07 and 0.1620±0.0004 ns, respectively.

Both in the channel and in the 2D QW, the recombination time first increases with increasing pump power. However, with a further increase in the pump power, the recombination time in the channel drops at a critical value of the pump power about 10 μW, which is not observed in the 2D QW. Similar behaviors is found for the inter-level transition time Δt obtained in the channel (the inset to figure 6(a)) and in the 2D QW (the inset to figure 6(b)). This is due to the fact that the time Δt is associated with electrons, which, like holes, contribute to the bipolar diffusion under study. Both, holes and electrons exhibit hydrodynamic properties. Therefore, similar features are expected for τ_{hh}, τ_{lh} and Δt.

The recombination rate is fundamentally influenced by the dynamics of electrons and holes, namely, their relative motion. In order to recombine, electrons and holes must occupy the same space which is determined by the coherence volume of excitons. The exciton coherence volume is determined by exciton scattering. As the pump power increases, the number of excitons increases, which enhances their mutual scattering. As theoretically predicted in [24], exciton–exciton scattering leads to a linear increase in the uniform broadening of the exciton state with increasing pump power, which reduces the rate of their recombination [25]. Therefore, increasing pump power causes rise of the recombination time. The recombination time, which increases with increasing pump power was observed in GaAs and CdTe QWs in [26, 27].

Thus, an increase in the recombination time both in the channel and in the 2D QW with increasing pump power is associated with a corresponding decrease in the exciton coherence volume due to exciton–exciton scattering. However, at about 10 μW, the recombination time in the channel begins to decrease, while in the 2D QW it continues to increase with increasing pump power. Below we will demonstrate that such a remarkable behavior of the recombination time found in the mesoscopic channel is due to the hydrodynamic properties of the electron–hole plasma.

In the sample studied here, particular scattering conditions, when electron–electron collisions dominate over collisions of electrons with disorder (static random potential or phonons), provide for a viscous electron flow [19]. In a mesoscopic channel of width W >> l_{ee} such viscous electrons form a Hagen–Poiseuille charge flow with a non-uniform diffusion velocity profile [12]. The inhomogeneous Poiseuille flow diffusion velocity profile gives rise to the case when carriers with different velocities are influenced by the surface recombination in a different way. Rapid carriers moving in the middle of the channel are less affected by the surface recombination and therefore, they have longer lifetime as compared to the slow carriers close to the channel boundary. What is more, the measured PL intensity is collected from an area with a size equal to the diffusion length of photogenerated carriers. In the mesoscopic channel under study, the diffusion lengths of both heavy and light holes are equal to or larger than the channel width. Therefore, the measured recombination time is averaged over the channel width. In the case of the Poiseuille

flow, the long lifetime of fast carriers dominates the total recombination time measured by the time-resolved PL. At the same time, for the Drude diffusive regime, the almost uniform diffusion velocity profile increases the fraction of the carriers recombining near the boundary. As a result, in this case, the total recombination time decreases. As the pump power increases, the character of the diffusion flow is affected by the dissipative scattering of electrons by slow photogenerated holes. At the critical pump power, when l_{ee} becomes comparable or greater than the mean free path related to electron–hole scattering, the Poiseuille flow becomes a homogeneous diffusion flow. According to the above explanation, this leads to a decrease in the recombination time. The velocity profiles corresponding to different pump power are schematically shown in the inset to figure 6(a).

The critical pump power, when electron–hole scattering becomes dominant over electron–electron scattering, is indicated in figure 6(a) by a vertical dashed line. Thus, the influence of the shape of the diffusion velocity profile on the recombination time explains the decrease in the recombination time measured in the mesoscopic channel with increasing pump power. This in turn, shows that the dependence of the recombination time on the pump power points to a character of the particle flow. In the case in question, the maximum recombination time observed with increasing pump power indicates a transition from the viscous to the diffusive regime of the electron–hole plasma. This transition occurs both in the mesoscopic channel and in the 2D GaAs QW. However, the presence of boundaries makes the transition from the viscous to the diffusive regime much more pronounced: in the channel, it causes the maximum recombination time at the critical pump power, while at the same pump power in the 2D QW, only a weak kick is detected in the dependence of the recombination time on the pump power.

As a final point, provided determination of the diffusion lengths and the lifetimes individually, the ambipolar diffusion coefficients related to heavy and light holes $D_{hh} \simeq 0.17\,m^2\,s^{-1}$ and $D_{lh} \simeq 0.3\,m^2\,s^{-1}$, respectively, were determined in the viscose regime. Nearly equal diffusion coefficients associated with heavy and light holes mean that both type of holes, together with electrons form a single three-component hydrodynamic system.

Furthermore, the above-discussed effect of pump power on the recombination time resembles what happens to the conductivity as a function of temperature in accordance with the Gurzhi effect which was predicted to occur in metallic electron systems when the mean free path for interelectronic scattering l_{ee} is much smaller than both the device length W and the mean momentum relaxation free path l_p. If the scattering on the sample edges is diffusive, the electron transport is controlled by the relation between l_{ee} and W: when $l_{ee} << W$ the scattering at the edges provides the momentum loss and the electron transport resembles the Poiseuille flow with the resistance decreasing quadratically with increasing temperature [6]. In both cases of the Gurzhi effect and the observed decrease in the recombination time with increasing pump power, the decisive role is played by the inhomogeneity of the Poiseuille charge flow in the channel, when the temperature dependence of the conductivity is determined by scattering at the boundary roughness, while the dependence of the recombination time on the pump power is determined by surface recombination at the boundary.

4. Conclusion

The recombination dynamics was studied in viscous electron–hole plasma consisting of electrons and photogenerated heavy and light holes, formed in high mobility mesoscopic GaAs channel. The observed biexponential PL decay indicates the independent character of the recombination of photogenerated heavy and light holes with background electrons. An unusual behavior of the recombination time with increasing pump power was found: first, the recombination time increases, and then, at a critical pump power, the recombination time begins to decrease. The observed increase in the recombination time is attributed to the corresponding decrease in the concentration and mobility of background electrons. At a critical pump power the scattering of electrons with disorder begins to dominate over electron–electron scattering. Consequently, the Poiseuille inhomogeneous charge flow is transformed into an nearly uniform Drude diffusive flow, which increases the fraction of carriers that rapidly recombine near the channel boundary. As a result, the measured average recombination time decreases. Thus, a transition from the viscous to the diffusive regime of a hydrodynamic electron–hole plasma has been discovered.

Data availability statement

The data that support the findings of this study are available upon reasonable request from the authors.

Acknowledgments

Financial supports from the Brazilian agencies FAPESP (Grant 2022/02132-0), CNPq (Grant 301013/2019-5) are gratefully acknowledged.

ORCID iDs

Yu A Pusep https://orcid.org/0000-0001-8501-0838
M A T Patricio https://orcid.org/0000-0003-4187-1825
G M Jacobsen https://orcid.org/0000-0001-6364-4549
G M Gusev https://orcid.org/0000-0003-3646-6024

References

[1] Jungel A 2001 *Quasi-Hydrodynamic Semiconductor Equations* (Basel: Birkauser Verlag)
[2] Conti S and Vignale G 1999 *Phys. Rev.* B **60** 7966
[3] Govorov A O and Heremans J J 2004 *Phys. Rev. Lett.* **92** 026803
[4] Andreev A V, Kivelson S A and Spivak B 2011 *Phys. Rev. Lett.* **106** 256804
[5] Polini M and Geim A K 2020 *Phys. Today* **73** 28

[6] Gurzhi R N 1963 *J. Exp. Theor. Phys.* **17** 521
[7] Molenkamp L W and de Jong M J M 1994 *Phys. Rev.* B **49** 5038
[8] de Jong M J M and Molenkamp L W 1995 *Phys. Rev.* B **51** 13389
[9] Gurzhi R N, Kalinenko A N and Kopeliovich A I 1995 *Phys. Rev. Lett.* **74** 3872
[10] Predel H, Buhmann H, Molenkamp L W, Gurzhi R N, Kalinenko A N, Kopeliovich A I and Yanovsky A V 2000 *Phys. Rev.* B **62** 2057
[11] Alekseev P S 2016 *Phys. Rev. Lett.* **117** 166601
[12] Bandurin D A *et al* 2016 *Science* **351** 1055
[13] Levitov L and Falkovich G 2016 *Nat. Phys.* **12** 672
[14] Moll P J W, Kushwaha P, Nandi N, Schmidt B and Mackenzie A P 2016 *Science* **351** 1061
[15] Gusev G M, Levin A D, Levinson E V and Bakarov A K 2018 *AIP Adv.* **8** 025318
[16] Alekseev P S and Alekseeva A P 2019 *Phys. Rev. Lett.* **123** 236801
[17] Keser A C V *et al* 2021 *Phys. Rev.* X **11** 031030
[18] Svintsov D, Vyurkov V, Yurchenko S, Otsuji T and Ryzhii V 2012 *J. Appl. Phys.* **111** 083715
[19] Pusep Y A, Teodoro M D, Laurindo Jr. V, de Oliveira E R C, Gusev G M and Bakarov A K 2022 *Phys. Rev. Lett.* **128** 136801
[20] Kiselev E I and Schmalian J 2019 *Phys. Rev.* B **99** 035430
[21] Lyo S K and Jones E D 1988 *Phys. Rev.* B **38** 4113
[22] Alekseev P S and Dmitriev A P 2020 *Phys. Rev.* B **102** 241409(R)
[23] Bastard G 1988 *Wave Mechanics Applied to Semiconductor Heterostructures* (New York: Halsted)
[24] Manzke G, Henneberger K and May V 1987 *Phys. Status Solidi* b **139** 233
[25] Feldmann J, Peter G, Gobel E O, Dawson P, Moore K, Foxon C and Elliott R J 1987 *Phys. Rev. Lett.* **59** 2337
[26] Eccleston R, Feuerbacher B F, Kuhl J, Ruhle W W and Ploog K 1992 *Phys. Rev.* B **45** 11403
[27] O'Neill M, Oestreich M, Ruhle W W and Ashenford D E 1993 *Phys. Rev.* B **48** 8980